

Isomer-Specific Ultraviolet Spectroscopy of *m*- and *p*-Divinylbenzene[†]Talitha M. Selby,[‡] W. Leo Meerts,[§] and Timothy S. Zwier^{*,‡}

Department of Chemistry, Purdue University, West Lafayette, Indiana 47907-2084, and Molecular and Biophysics Group, Institute for Molecules and Materials, Radboud University Nijmegen, P.O. Box 9010, NL-6500 GL Nijmegen, The Netherlands

Received: December 1, 2006; In Final Form: January 22, 2007

The ultraviolet spectroscopy of *m*- and *p*-divinylbenzene isomers (*m*DVB and *p*DVB) was studied by a combination of methods, including resonance-enhanced two-photon ionization (R2PI), laser-induced fluorescence (LIF), UV–UV hole-burning spectroscopy (UVHB), and single vibronic level fluorescence spectroscopy (SVLF). In *m*DVB, there are three low-energy conformations, *cis*–*cis*, *cis*–*trans*, and *trans*–*trans* whose $S_1 \leftarrow S_0$ origins occur at 31 408, 31 856, and 32 164 cm^{-1} , respectively, as confirmed by UVHB spectroscopy. There are two possible conformations in *p*DVB, *cis* and *trans*. UVHB studies confirm the $S_1 \leftarrow S_0$ origin of *trans*-*p*DVB occurs at 32 553 cm^{-1} , and the corresponding *cis*-*p*DVB origin is tentatively assigned to a transition at 32 621 cm^{-1} . SVLF studies were used to determine several of the vinyl torsional levels of the isomers of *m*DVB and *p*DVB. A two-dimensional flexible model was used to fit these levels in *m*DVB to a potential form and determine the barriers to isomerization.

I. Introduction

Styrene (STY) and substituted styrenes are ideal model systems for studying photoinduced *cis*–*trans* isomerization processes. The reaction coordinate associated with isomerization involves internal rotation about the C_1 – C_α bond that connects the ring to the vinyl group. The vinyl torsional energy levels thus map along the reaction coordinate and can be used to determine the one-dimensional potential for isomerization. Studies of the vibronic spectroscopy are particularly fruitful in this regard because the vibronic spectra of STY and its derivatives show characteristic Franck–Condon activity involving the vinyl torsion (ν_{42} in STY). STY is planar in both the ground and first excited electronic states.^{1–4} The torsion is very floppy in the ground state with a frequency of only 38 cm^{-1} .^{1–3} This results in part because the ground state torsional potential well is very flat-bottomed, giving rise to a large negative anharmonicity for low quantum numbers.^{1–3} However, in the $S_1(\pi\pi^*)$ excited state, the C_1 – C_α bond length decreases as it gains double bond character and the C=C vinyl bond lengthens as it loses double bond character, causing the torsional potential well to become much steeper and the frequency of the torsion to increase to 186 cm^{-1} .^{2,4} The differences in the shapes of the ground and excited state potential wells lead to a short progression of even quanta in the vinyl torsion in the low-frequency region of the 0^0_0 SVLF spectrum of STY.^{2,3} The changes in bonding character in the excited state also cause the normal coordinates of the out-of-plane (oop) bend and torsion (Q_{41} and Q_{42} , respectively) to mix.^{2,3} Thus, these coordinates in the excited state must be expressed as linear combinations of the ground state bending and torsional normal mode coordinates.^{2,3} This mixing of normal coordinates is referred to as a Duschinsky rotation because the normal mode axes are

rotated in $3N - 6$ dimensional space with respect to one another. As a result of this mixing, the Franck–Condon factors (FCF) in the $S_1 \leftarrow S_0$ excitation spectrum are spread out over both the “torsion” and “bending” modes.⁵

The barrier to isomerization of the vinyl group in the ground state of STY was determined by Hollas and co-workers³ by fitting the observed ground state torsional levels to a Fourier series,

$$V(\theta) = \sum_n \frac{1}{2} V_n (1 - \cos(n\theta))$$

The best fit of the experimental data was achieved with the following functional form,³

$$V(\theta) = \frac{1}{2} [(1070 \pm 8)(1 - \cos(2\theta)) - (275 \pm 1)(1 - \cos(4\theta)) + (7 \pm 0.5)(1 - \cos(6\theta))]$$

The value of the torsional barrier height ($1070 \pm 8 \text{ cm}^{-1}$) in this potential is determined by the V_2 term. The large negative value of the V_4 term reflects the flatness of the potential well, and the V_6 term provides mainly a small correction to the shape of the well.

In the spirit of exploring potential energy surfaces of increasing complexity,^{6–9} we have extended our recent studies⁷ of *m*- and *p*-ethynylstyrene that possess one flexible vinyl coordinate to *m*- and *p*-divinylbenzene, which contain two such coordinates. With the vinyl group’s inherent structural asymmetry, this double substitution also produces more isomeric possibilities. As shown in Figure 1, in *p*DVB, one anticipates two isomers with vinyl groups pointing *cis* and *trans* relative to one another, and in *m*DVB there are three isomers: *cis*–*cis* (*cc*), *trans*–*trans* (*tt*), and *cis*–*trans* (*ct*). *Trans*–*cis* is spectroscopically indistinguishable from *cis*–*trans*.

The laser induced fluorescence spectrum of *m*- and *p*DVB was first recorded by Nguyen and co-workers.¹⁰ High-resolution fluorescence excitation spectra of many of the major transitions

[†] Part of the special issue “James A. Miller Festschrift”.

^{*} Corresponding author. E-mail: zwier@purdue.edu. Phone: (765) 494-5278. Fax: (765) 494-5330.

[‡] Purdue University.

[§] Radboud University Nijmegen.

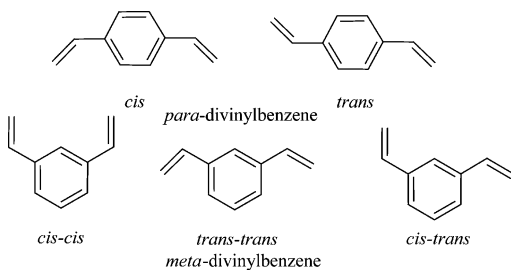


Figure 1. Depictions of the DVB conformers.

were also recorded. Surprisingly, only two *meta*-conformers (*cc* and *tt*) and one *para*-conformer (*t*) were identified. Thus, *ct*-*m*DVB and *c*-*p*DVB were not found in the spectrum. The origins of *cc*-*m*DVB, *tt*-*m*DVB, and *t*-*p*DVB were identified at 31 409, 32 164, and 32 553 cm^{-1} , respectively.

The purposes of the present study are to find the “missing” conformations of *m*- and *p*DVB, to characterize the conformation specific ultraviolet spectroscopy of all the isomers in both the ground and excited electronic states, and to determine the barrier to *cis* \leftrightarrow *trans* isomerization by fitting the $\text{C}_1\text{--C}_\alpha$ torsional levels to a two-dimensional potential form. This involves a long extrapolation of the low-frequency torsional levels to the top of the barrier, leaving some uncertainty as to the accuracy of such an extrapolation. Furthermore, such a spectroscopic study cannot identify isomerization pathways on the surface. In the following paper, we determine the lowest-energy isomerization barriers between all six reactant–product pairs of *m*DVB using the alternative method of stimulated emission pumping–population transfer spectroscopy.^{6,7,11,12} This enables a comparison of the purely spectroscopic methods for determining barrier heights with the population transfer methodology.

II. Experimental Methods

Ultraviolet excitation spectra were obtained with both laser induced fluorescence (LIF) and resonance enhanced two photon ionization (R2PI) detection schemes. The chamber used for ionization detection has been previously described.¹³ In this chamber, the supersonic expansion was produced by passing He over a sample reservoir heated to about 50 °C. A total pressure of 2 bar was applied behind a pulsed valve (Jordan Co.) with a 0.8 mm diameter orifice.

The LIF chamber used in this work is newly designed, and it will be described in more detail elsewhere. This apparatus consists of a six-way cross chamber backed by a roots pump (Leybold, model WS 100) and two 25 L/s mechanical pumps (Sargent-Welch, model 1398). The fluorescence is collected with $\sim 20\%$ efficiency with 4 in. spherical mirrors^{14,15} and imaged onto a photomultiplier tube (PMT). In LIF experiments, the sample was entrained in ~ 3 bar helium and expanded into vacuum by a pulsed valve (Series 9 general valve) with a 1 mm nozzle at a throughput of $\sim 60 \text{ bar}\cdot\text{cm}^3/\text{min}$.

In both detection schemes, the frequency doubled output from a Nd:YAG pumped dye laser was used as the excitation laser. The excitation laser powers used were ~ 0.2 and $\sim 0.05\text{--}0.1$ mJ/pulse at 20 Hz in R2PI and LIF experiments, respectively.

To obtain conformer specific ultraviolet spectra, a high powered holeburn laser with its wavelength fixed on a vibronic band of interest (~ 0.4 mJ/pulse at 10 Hz) was introduced prior to the probe laser. When the probe laser was resonant with a transition that shared the same ground state as the holeburn transition, a depletion in the signal from the probe laser was detected due to the presence of the holeburn laser. The holeburn

spectrum was recorded by tuning the probe laser through the spectral region of interest. When its signal with the holeburn laser present was subtracted from that without the holeburn laser using active baseline subtraction, the conformer-specific ultraviolet holeburn (UVHB) spectrum resulted. In R2PI detection, both beams were spatially overlapped and there was a 200 ns delay between the two lasers. In LIF detection, the holeburn laser preceded the probe laser by $\sim 2 \mu\text{s}$, and the two beams were separated in space by ~ 4 nozzle diameters (typically with the holeburn laser at $x/D \sim 10$ and the probe laser at $x/D \sim 14$, where $D = 1.0 \text{ mm}$). In LIF detection, a gating circuit was used to turn off the PMT during the firing of the holeburn laser. The gating circuit was used to avoid saturation of the PMT from the holeburn laser.

Ground state vibrational spectra were recorded with single vibronic level fluorescence (SVLF) experiments. Here the excitation laser power used was $\sim 0.1\text{--}0.4$ mJ/pulse at 20 Hz. These spectra were recorded in the collision free region of the jet at $x/D \sim 14$. The total fluorescence was dispersed using a Jobin Yvon 750i monochromator with a 100 μm slit width equipped with a 1200 grooves/mm grating. The dispersed fluorescence signal was detected with a thermoelectrically cooled ($-75 \text{ }^\circ\text{C}$) CCD camera (Andor Technology) equipped with a 2048 \times 512 pixel chip with 13 μm diameter pixels. This signal was transferred directly to a personal computer. Background and scattered light were removed from the SVLF spectra by acquiring spectra while tuned out of the gas pulse and subtracting the two spectra.

The divinylbenzene sample was purchased from Aldrich as an 80 vol % mixture of *m*- and *p*-divinylbenzene isomers (the remainder *m*- and *p*-ethylstyrene) and used without purification.

III. Calculations

Density functional theory (DFT) calculations with a Becke3LYP functional^{16,17} and the 6-31+G* basis set¹⁸ were used to determine structures, energies, and harmonic vibrational frequencies for each of the isomers of DVB. True minima were verified by the lack of imaginary frequencies in the harmonic vibrational frequency calculations. All computations were carried out using the Gaussian 98 suite.¹⁹

In order to guide our thinking and to compare with experiment, the two-dimensional torsional potential for *m*DVB was computed at the DFT/B3LYP//6-31+G* level of theory. This is a relaxed potential energy surface in that at each set of torsional angles (θ_1, θ_2) the energy was minimized with respect to all other coordinates. The computed relaxed potential energy surface in the $0\text{--}\pi$ range for both θ_1 and θ_2 is shown in Figure 2. The four minima and the C_2 symmetry transition state are labeled in the figure. The dihedrals θ_1 and θ_2 are defined with $\theta_1 = \theta_2 = 0$ set at the *cis*–*cis* configuration. Positive angular change along either dihedral is defined as a counterclockwise rotation of the vinyl group when viewed from the center-of-mass along the $\text{C}(\phi)\text{--C}(\text{vinyl})$ bond. Because the two vinyl groups are identical and are attached at symmetry-equivalent points on a planar scaffold (the phenyl ring), the potential must be symmetric with respect to exchange of the torsional coordinates; that is, $V(\theta_1, \theta_2) = V(\theta_2, \theta_1)$. Table 1 lists the computed relative energies of the minima and transition states.

Figure 3 illustrates the normal coordinate displacements for the out-of-plane torsions in the three isomers of *m*DVB. In *ct*-*m*DVB (C_s symmetry), the two torsions are largely localized on the two different vinyl groups, which are distinguishable in this case. In contrast, in *cc*- and *tt*-*m*DVB (due to their C_{2v}

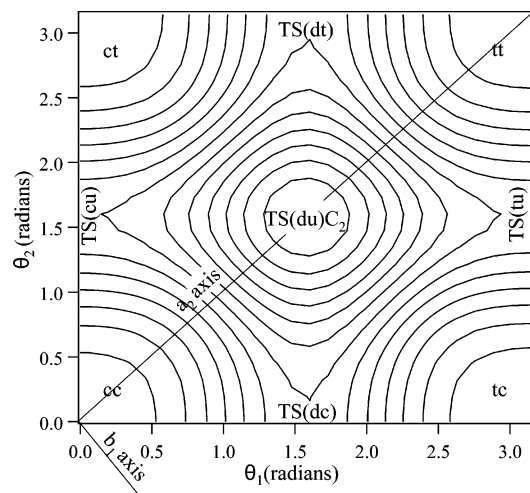


Figure 2. DFT relaxed potential energy surface in the $0-\pi$ range of *m*DVB with the minima, transition states, and symmetry axes labeled. See text for the energies of the minima and transition states. The two-letter labels indicate the orientation of the two vinyl groups where “c”= cis, “u”= up, “t”= trans, and “d”= down. See text for details.

TABLE 1: DFT/B3LYP//6-31+G* Relative Energies of Selected Stationary Points on the Potential Energy Surface of *m*-Divinylbenzene

description	θ_1 (deg)	θ_2 (deg)	relative energy (cm^{-1}) ^a
<i>tt</i> - <i>m</i> DVB	180	180	0
<i>ct</i> - <i>m</i> DVB	0	180	18
<i>cc</i> - <i>m</i> DVB	0	0	75
1D TS (<i>tu</i> , <i>dt</i>)	90	180	1274
1D TS (<i>cu</i> , <i>dc</i>)	0	90	1283
2D TS (<i>du</i>)	90	90	2590

^a The relative energies of the minima and transition states are corrected for zero-point energy effects.

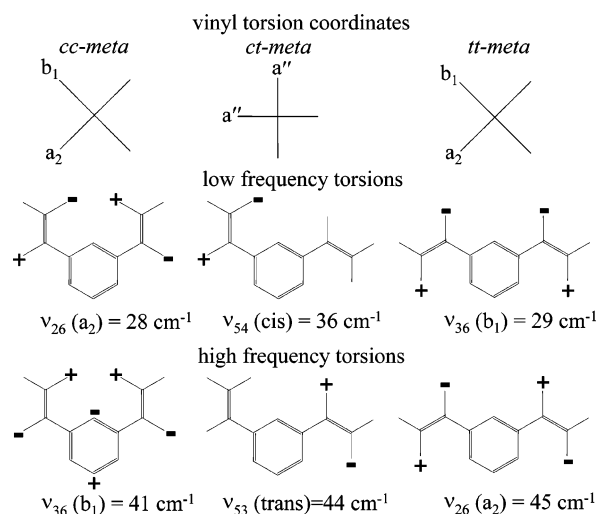


Figure 3. Illustration of the normal coordinate displacements in the isomers of *m*DVB with DFT frequencies. The DFT/B3LYP//6-31+G* frequencies are scaled by 0.9565.

symmetries) the two vinyl groups are both equally involved in the normal modes, and the normal coordinates are rotated by $\pm 45^\circ$ from the *ct*-conformer. As illustrated in the bottom of Figure 3, the higher frequency torsion in *cc*-*m*DVB has b_1 symmetry, whereas in *tt*-*m*DVB, it has a_2 symmetry. Additionally, the forms of the b_1 torsional modes in *cc*- and *tt*-*m*DVB are slightly different. As shown in Figure 2, in *cc*-*m*DVB in addition to the vinyl group motion, there is also significant

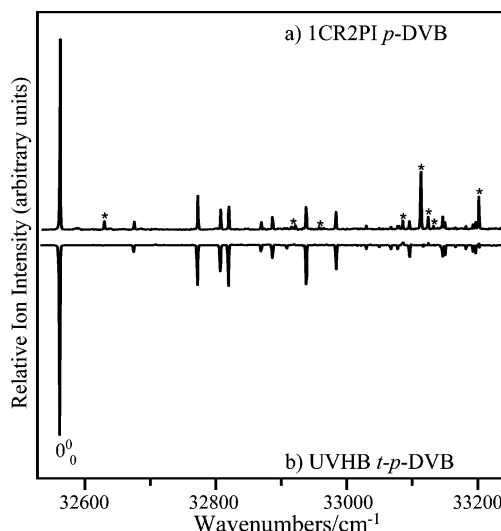


Figure 4. (a) 1C-R2PI spectrum of *p*DVB and (b) UVHB spectrum of *t*-*p*DVB. Transitions marked with asterisks in (a) represent transitions that do not holeburn out with *t*-*p*DVB. These transitions are tentatively assigned to transitions of *c*-*p*DVB (see text for details).

displacement of the two ring carbon atoms that lie in the C_2 axis of the molecule. This is largely a kinematic effect associated with both vinyl groups extending in the same direction from the ring. This motion appears as a tilt of the ring with respect to the vinyl groups. The corresponding displacement is not observed in *tt*-*m*DVB. However, it is present in *ct*-*m*DVB but to a smaller degree. Interestingly, in *ct*-*m*DVB, this displacement is larger for the lower frequency vibration where the vibration is localized on the “cis” side of the molecule.

The other low-frequency vibration of particular relevance to this study is the out-of-plane vinyl bending modes. Unlike the vinyl torsions, the normal coordinates of the bending modes of all isomers are delocalized over both vinyl groups. Furthermore, the lower frequency bend in all conformers correspond to the bending motion of both groups together (a “ b_1 ”-type or “in-phase” vibration).

IV. Results and Analysis

1. R2PI, LIF, and UVHB Spectra. *p*DVB. Parts a and b of Figure 4 present the 1C-R2PI spectrum of *p*DVB and the UVHB spectrum of *t*-*p*DVB in the range from 32 540 to 33 250 cm^{-1} . The ultraviolet spectrum (Figure 4a) of *p*DVB could be recorded free from interference from *m*DVB using 1C-R2PI because only the *p*DVB isomer has an ionization potential low enough to be reached by two photons of the same energy at these wavelengths.

The strongest transition in the R2PI spectrum occurs at 32 553 cm^{-1} (Figure 4a). This band was assigned by Nguyen and co-workers¹⁰ to the $S_1 \leftarrow S_0$ origin transition of *t*-*p*DVB. The UVHB spectrum of *t*-*p*DVB (Figure 4b) was recorded with the excitation laser fixed on the 0^0_0 *t*-*p*DVB transition. There are several transitions which do not holeburn out with the 0^0_0 transition of *t*-*p*DVB (marked by asterisks in Figure 4). By process of elimination, these transitions are tentatively assigned to the missing *c*-*p*DVB conformer. Further evidence for the assignment of these transitions belonging to *c*-*p*DVB will be discussed below. The furthest red-shifted transition of these unaccounted for transitions, which occurs at 32 621 cm^{-1} , is tentatively assigned to the 0^0_0 transition of *c*-*p*DVB.

***m*DVB.** Figure 5 presents the LIF spectrum of *m*DVB (part a of Figure 5) and the UVHB spectra of *cc*-, *ct*-, and *tt*-

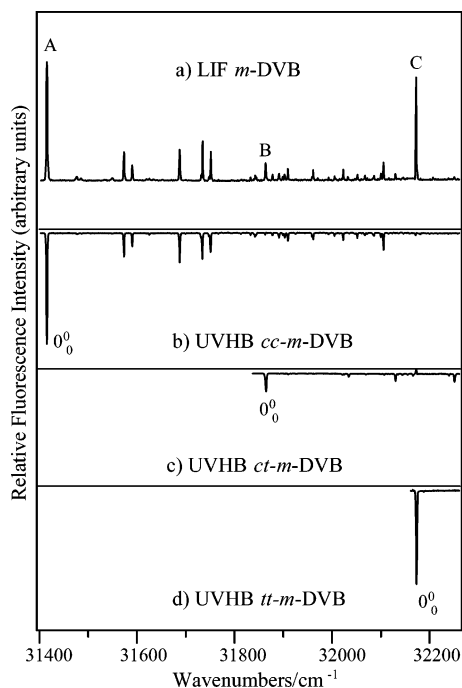


Figure 5. (a) LIF spectrum of *mDVB* and UVHB spectra of (b) *cc*-, (c) *ct*-, and (d) *tt*-*mDVB* with their origin transitions labeled.

mDVB (parts b, c, and d of Figure 5, respectively) in the range of 31 400 to 32 300 cm^{-1} . The spectrum shown in Figure 5a is very similar to the LIF spectrum recorded by Nguyen and co-workers.¹⁰ Some intensity differences are observed, which are probably due to differences in the laser powers used.

The two strongest transitions, labeled A and C, in the LIF spectrum occur at 31 409 and 32 164 cm^{-1} (Figure 5a). These bands were assigned by Nguyen and co-workers¹⁰ to the $S_1 \leftarrow S_0$ origin transitions of *cc*- and *tt*-*mDVB*, respectively, based on their rotationally resolved spectra. The UVHB spectra of *cc*- and *tt*-*mDVB* (parts b and d of Figure 5) do not account for all transitions observed in the LIF spectrum. However, all of the unaccounted for transitions do holeburn out with the furthest red-shifted transition of the unaccounted for peaks (Figure 5c). This third species has its origin at 31 856 cm^{-1} , in the position

where the *ct*-*mDVB* origin is expected to occur, roughly halfway between those of the *cc*- and *tt*- isomers.⁸ Stimulated-emission population transfer studies (which will be discussed in the following paper) confirm that the third species is *ct*-*mDVB*.

Given the small intensity of the *ct*-*mDVB* and *c*-*pDVB* transitions relative to the other *m*- and *pDVB* conformers, it is understandable that these conformers were missed in the previous studies of the divinylbenzenes by Nguyen and co-workers.¹⁰ Furthermore, only the strongest two transitions (at 33 105 and 33 193 cm^{-1}) of all the *c*-*pDVB* transitions can be clearly seen in the LIF spectrum (not shown), and the LIF intensities of these two transitions are only about one-fifth of the R2PI intensity relative to the *t*-*pDVB* origin transition. The fact that the transitions due to *c*-*pDVB* transitions are so much more easily detected using R2PI than LIF is the result of the higher laser powers used in the R2PI spectroscopy (leading to saturation effects). In addition, the isomers of *pDVB* have significantly shorter S_1 lifetimes (~ 20 ns) than *mDVB* (~ 80 ns). Unfortunately, the lifetime of *c*-*pDVB* transitions could not be determined because the two observed transitions are both partially overlapped with transitions of the *mDVB* conformers, which have long lifetimes.

2. Ground and Excited State Vibrational Assignments.

Figures 6 and 7 present the UVHB and 0^0_0 SVLF spectra of *cc*-, *ct*-, *tt*-*mDVB* and *t*-*pDVB*, respectively, plotted in wavenumbers relative to their respective $S_1 \leftarrow S_0$ origin transitions. Assignments for the vibronic transitions are given in the figures and in Tables 2 and 3. The normal modes are numbered using Mulliken notation, based on the harmonic vibrational frequencies from DFT calculations. Support for these assignments and a general discussion of the most important bands are given in what follows. The *cc*-*mDVB* spectra will be discussed in greater detail in order to illustrate the assignment process used.

cc-*mDVB*. As expected from the high-resolution spectroscopy by Nguyen et al.,¹⁰ the $S_1 \leftarrow S_0$ excitation (Figure 6a) and 0^0_0 SVLF (Figure 7a) spectra are dominated by a_1 fundamentals and even overtones and combinations of oop vibrations of the same symmetry (a_2 and b_1). Frequencies of *cc*-*mDVB* fundamentals are given in Table 2 alongside DFT calculated frequencies and the corresponding ground and excited state frequencies observed in STY for comparison.

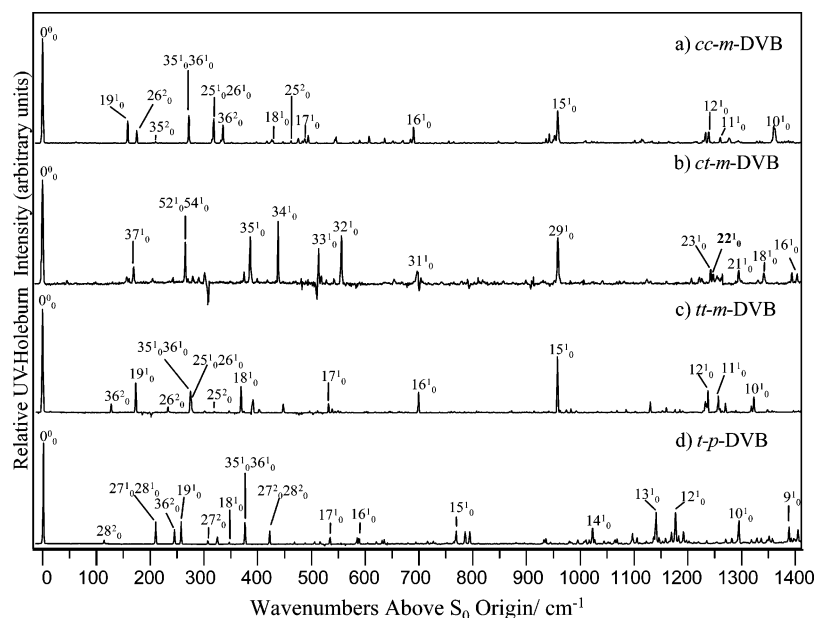


Figure 6. UVHB spectra of (a) *cc*-*mDVB*, (b) *ct*-*mDVB*, (c) *tt*-*mDVB*, and (d) *t*-*pDVB* in wavenumbers relative to the respective origin transitions with many important transitions labeled. For comparison, the spectra have been scaled to the same 0^0_0 intensity.

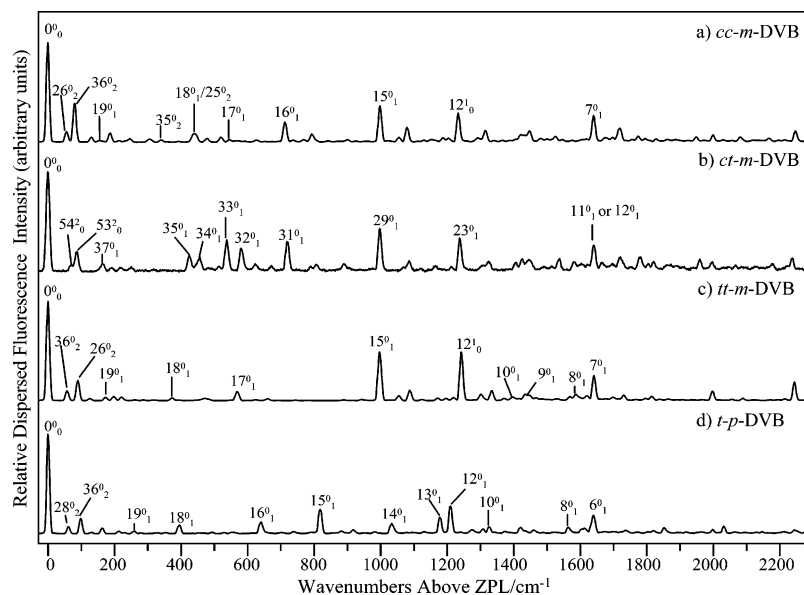


Figure 7. SVLF spectra from the 0^0_0 transitions of (a) *cc*-*m*DVB, (b) *ct*-*m*DVB, (c) *tt*-*m*DVB, and (d) *t*-*p*DVB in wavenumbers above the ZPL with many important transitions labeled. Each spectrum is normalized such that the 0^0_0 intensity is 1.

TABLE 2: Experimental Ground and Excited State Vibrations of *cc*-*m*DVB and *tt*-*m*DVB with Styrene Vibrations² Shown for Comparison

styrene		<i>cc</i> - <i>m</i> DVB						
description ^a	mode	S ₀ frequency (cm ⁻¹)	S ₁ frequency (cm ⁻¹)	symmetry	mode	S ₀ frequency (cm ⁻¹)	S ₁ frequency (cm ⁻¹)	S ₀ calcd ^b (cm ⁻¹)
ν C=C	9	1630		a ₁	7	1640		1627
ϕ - ν CC	11	1575		a ₁	8	1527		1554
ϕ - ν CC	13	1450	1429	a ₁	9	1448	1431 ^d	1425
β -CH ₂	14	1411		a ₁	10	1422	1360 ^d	1405
ϕ - β CH	15	1334		a ₁	11		1260 ^d	1292
ϕ - ν CC/(13)	18	1203	1209	a ₁	12	1232	1240	1205
ϕ -deform/(12)	24	1001	948	a ₁	15	998	958	968
ϕ -breath/1	25	775	746	a ₁	16	713	690	696
α C-C-C	27	553	437	a ₁	17	547		528
α C-C-C/(6a)	28	437	394	a ₁	18	441	429 ^d	434
β C-CHCH ₂	29	228	237	a ₁	19	155	158	152
C1-C α bend ^c	41	199	99	a ₂	25	220	231	221
C1-C α torsion ^c	42	38	186	a ₂	26	28	88	34
C1-C α bend ^c	41	199	99	b ₁	35	171	105	173
C1-C α torsion ^c	42	38	186	b ₁	36	41	168	48

styrene		<i>tt</i> - <i>m</i> DVB						
description ^a	mode	S ₀ frequency (cm ⁻¹)	S ₁ frequency (cm ⁻¹)	symmetry	mode	S ₀ frequency (cm ⁻¹)	S ₁ frequency (cm ⁻¹)	S ₀ calcd ^b (cm ⁻¹)
ν C=C	9	1630		a ₁	7	1641		1628
ϕ - ν CC	11	1575		a ₁	8	1588		1560
ϕ - ν CC	13	1450	1429	a ₁	9	1439	1427 ^d	1424
β -CH ₂	14	1411		a ₁	10	1397	1322 ^d	1373
ϕ - β CH	15	1334		a ₁	11	1295	1257	1291
ϕ - ν CC/(13)	18	1203	1209	a ₁	12	1243	1237	1214
ϕ -deform/(12)	24	1001	948	a ₁	15	997	958	968
ϕ -breath/1	25	775	746	a ₁	16	720	699	701
α C-C-C	27	553	437	a ₁	17	569	532	555
α C-C-C/(6a)	28	437	394	a ₁	18	373	369	363
β C-CHCH ₂	29	228	237	a ₁	19	171	174	165
C1-C α bend ^c	41	199	99	a ₂	25	198	160	198
C1-C α torsion ^c	42	38	186	a ₂	26	45	116	55
C1-C α bend ^c	41	199	99	b ₁	35	192	210	197
C1-C α torsion ^c	42	38	186	b ₁	36	29	64	35

^a ν , stretch; α , in plane ring angle bend; β , in plane bend; ϕ , benzene ring. Numbers in parentheses refer to corresponding benzene mode in Wilson notation. ^b DFT/B3LYP//6-31+G* level of theory. ^c Estimated fundamental from combinations or overtones observed assuming harmonic behavior. See text for details. ^d Assignments are tentative.

Firm assignments to the transitions located at 158, 690, 958, and 1240 cm⁻¹ above the S₀ ← S₁ origin were made to transitions involving a₁ fundamentals, 19¹₀, 16¹₀, 15¹₀, and 12¹₀,

respectively, based on their SVLF spectra. These scans are included in the Supporting Information. The largest of these transitions, 15¹₀, at 958 cm⁻¹ involves ν_{15} , a ring deformation

TABLE 3: Ground and Excited State Vibrations of *t-p*DVB and *cc-m*DVB with Styrene Vibrations² Shown for Comparison

description ^a	styrene			symmetry	<i>t-p</i> DVB			
	mode	S ₀ frequency (cm ⁻¹)	S ₁ frequency (cm ⁻¹)		mode	S ₀ frequency (cm ⁻¹)	S ₁ frequency (cm ⁻¹)	S ₀ calcd ^b (cm ⁻¹)
ν C=C	9	1630		a _g	6	1640		1621
ϕ - ν CC	11	1575		a _g	8	1564		1533
β -CH ₂	14	1411		a _g	9	1431 ^d	1388 ^d	1405
ϕ - β CH	15	1334		a _g	10	1327	1295	1311
ϕ - ν CC/(13)	18	1203	1209	a _g	12	1210	1177	1189
ν C1C α /aryl β CH	19	1181	966	a _g	13	1179	1141	1159
β CH ₂	22	1032		a _g	14	1033	1023	1013
ϕ -breath/1	25	775	746	a _g	15	817	769	795
ϕ - α C-C-C/(6b)	26	621	545	a _g	16	641	589 ^d	627
α C-C-C	27	553	437	a _g	17		535 ^d	537
α C-C-C/(6a)	28	437	394	a _g	18	394	347 ^d	384
β C-CHCH ₂	29	228	237	a _g	19	259	258	247
C1-C α bend ^c	41	199	99	a _u	27	133	154	136
C1-C α torsion ^c	42	38	186	a _u	28	30	57	38
C1-C α bend ^c	41	199	99	b _g	35	283	254	283
C1-C α torsion ^c	42	38	186	b _g	36	49	123	60

description ^a	styrene			symmetry	<i>cc-m</i> DVB			
	mode	S ₀ frequency (cm ⁻¹)	S ₁ frequency (cm ⁻¹)		mode	S ₀ frequency (cm ⁻¹)	S ₁ frequency (cm ⁻¹)	S ₀ calcd ^b (cm ⁻¹)
ν C=C	9	1630		a'	11	1638 ^d		1626
ν C=C	9	1630		a'	12	1638 ^d		1625
ϕ - ν CC	13	1450	1429	a'	16		1403 ^d	1424
β -CH ₂	14	1411		a'	18		1341 ^d	1384
ϕ - ν CC	17	1289	1145	a'	21		1295 ^d	1290
ϕ - ν CC	17	1289	1145	a'	22		1247 ^d	1266
ϕ - ν CC/(13)	18	1203	1209	a'	23	1238	1242	1211
ϕ -deform/(12)	24	1001	948	a'	29	997	958	967
ϕ -breath/(1)	25	775	746	a'	31	719	697	700
ν C-C-C	27	553	437	a'	32	580	556 ^d	566
ν C-C-C	27	553	437	a'	33	538	513	522
ν C-C-C/(6a)	28	437	394	a'	34	455	438	443
ν C-C-C/(6a)	28	437	394	a'	35	425	386	416
β C-CHCH ₂	29	228	237	a'	37	165	169	160
C1-C α bend ^c	41	199	99	a''	51		145 ^d	213
C1-C α bend ^c	41	199	99	a''	52	181 ^d	188 ^d	186
C1-C α torsion ^c	42	38	186	a''	53	44	135 ^d	57
C1-C α torsion ^c	42	38	186	a''	54	36	79 ^e	47

^a ν , stretch; α , in plane ring angle bend; β , in plane bend; ϕ , benzene ring. Numbers in parentheses refer to corresponding benzene mode in Wilson notation. ^b DFT/B3LYP//6-31+G* level of theory. ^c Estimated fundamental from combinations or overtones observed assuming harmonic behavior. See text for details. ^d Assignments are tentative.

mode corresponding to ν_{24} in STY and ν_{12} in benzene. The corresponding 15^0_1 transition appears at 998 cm⁻¹, indicating that the ring deformation experiences a frequency decrease in the excited state similar to that in STY (see Table 2). The transition at 158 cm⁻¹ is assigned to 19^1_0 , where ν_{19} is the symmetric vinyl bending mode. The frequency of ν_{19} decreases only slightly in S₀ to 155 cm⁻¹. This mode corresponds to ν_{29} in STY, where it has ground and excited state frequencies of 228 and 237 cm⁻¹, respectively.² The large frequency difference between *cc-m*DVB and STY reflects the fact that the normal mode in *cc-m*DVB involves both vinyl groups. The transitions observed at 690 cm⁻¹ in the R2PI spectrum and 713 cm⁻¹ in the 0^0_0 SVLF spectrum are assigned to 16^1_0 and 16^0_1 , respectively, where ν_{16} is the ring breathing mode. The corresponding modes in STY and benzene are ν_{25} and ν_1 . Finally, the transition at 1240 cm⁻¹ is assigned to 12^1_0 , where ν_{12} is a ring deformation mode. The corresponding ground state transition, 12^0_1 , is observed at 1232 cm⁻¹. The analogous STY mode is ν_{18} (ν_{13} in benzene).

Combination bands involving these in-plane fundamentals are also evident in the spectra, most notably involving ν_{15} , ν_{19} , ν_{16} , and ν_{12} . Transitions ascribable to other in-plane fundamental transitions observed in the 0^0_0 SVLF spectrum involving modes ν_7 - ν_{10} were assigned based on DFT calculations and compari-

son of the observed frequencies and intensities to those of the corresponding transitions in the 0^0_0 SVLF spectrum of STY. SVLF spectra were taken from transitions observed at 1431, 1360, and 1260 cm⁻¹ in the excitation spectrum; however, at these excitation energies the SVLF spectra were too broad to assign. On the basis of comparison to STY and DFT calculations, these transitions are tentatively assigned to 9^1_0 , 10^1_0 , and 11^1_0 , respectively.

The remaining prominent features in the 0^0_0 SVLF and the S₁ ← S₀ spectra of *cc-m*DVB are composed of combinations or even overtones involving the oop vinyl torsion and bends (ν_{42} and ν_{41} in STY). As discussed previously, in *cc-m*DVB there are two vinyl bends (ν_{25} and ν_{35}) and two vinyl torsions (ν_{26} and ν_{36}) with a₂ and b₁ symmetry, respectively. As in STY, there is complicated Duschinsky mixing of these modes and a large negative anharmonicity in the torsions.¹⁻³ Because the torsional modes are closely related to the isomerization reaction coordinates, they will be discussed in more detail here. Their assignments were complicated by the Duschinsky mixing and large anharmonicities.

Parts a-c of Figure 8 present the SVLF spectra from the (a) 26^2_0 (at +175 cm⁻¹), (b) $25^1_0 26^1_0$ (at +319 cm⁻¹), and (c) 25^2_0 (at +462 cm⁻¹) transitions of *cc-m*DVB. These are the first overtone of the a₂-torsion, the combination band of the a₂-bend

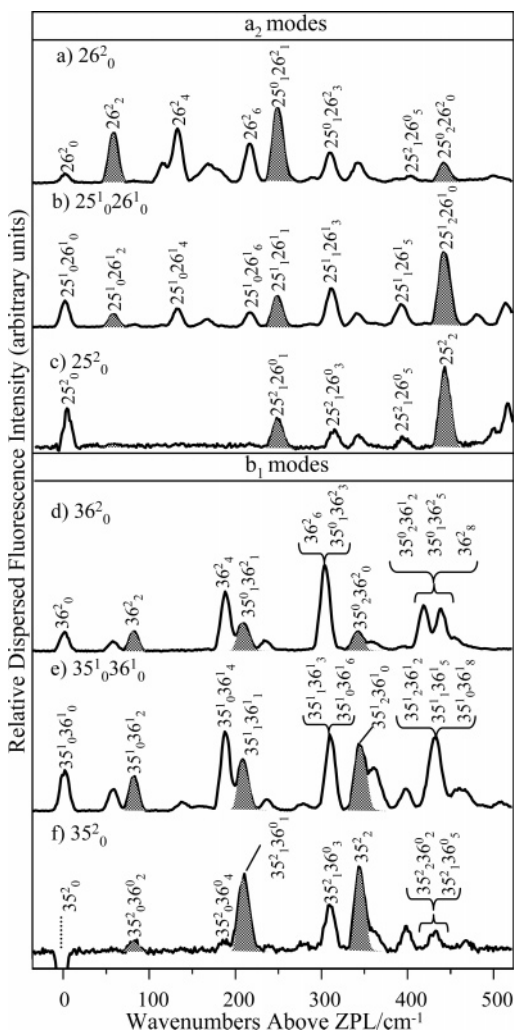


Figure 8. Assignments to out-of-plane vibrations observed in the SVLF of the (a) 26^2_0 (at $+175\text{ cm}^{-1}$), (b) $25^1_0 26^1_0$ (at $+319\text{ cm}^{-1}$), (c) 25^2_0 (at $+462\text{ cm}^{-1}$), (d) 36^2_0 (at $+336\text{ cm}^{-1}$), (e) $35^1_0 36^1_0$ (at $+272\text{ cm}^{-1}$), and (f) 35^2_0 (at $+210\text{ cm}^{-1}$) transitions of *cc*-*m*DVB.

and the a_2 -torsion, and the first overtone of the a_2 -bend, respectively. The frequencies of the assigned bands observed in these spectra are given in Table 4. These spectra share many transitions to the same ground state levels. The lowest frequency transition from 26^2_0 and $25^1_0 26^1_0$ occurs at 56 cm^{-1} in the ground state. This transition is assigned to $2\nu_{26}$, the lowest frequency mode predicted by DFT calculations, the a_2 -torsion. The next two common features in the SVLF spectra of 26^2_0 and $25^1_0 26^1_0$ are found at 130 and 214 cm^{-1} , and (by comparison to the anharmonicity of the torsion in STY)^{1–3} these are assigned to $4\nu_{26}$ and $6\nu_{26}$, respectively. The next fairly strong feature observed in all three SVLF spectra occurs at 439 cm^{-1} and is assigned to $2\nu_{25}$. This assignment is consistent with DFT calculations that predict ν_{25} , the a_2 -bend, to have a frequency of 221 cm^{-1} . Given that ν_{25} and ν_{26} are approximately 221 and 28 cm^{-1} , we expect $\nu_{25} + \nu_{26}$ will occur at approximately 249 cm^{-1} . This leads to the assignment of the fairly strong transition at 247 cm^{-1} observed in all three of the SVLF spectra to $\nu_{25} + \nu_{26}$. The two last common features in these SVLF spectra are observed at 308 and 390 cm^{-1} , which we assign to $\nu_{25} + 3\nu_{26}$ and $\nu_{25} + 5\nu_{26}$, respectively. These assignments are consistent with the anharmonicity observed in ν_{26} .

Given the intensities of cross-sequence bands in the SVLF spectra of 26^2_0 (at $+175\text{ cm}^{-1}$), $25^1_0 26^1_0$ (at $+319\text{ cm}^{-1}$), 25^2_0 (at $+462\text{ cm}^{-1}$), the Duschinsky mixing of ν_{25} and ν_{26} in the

excited state is quite obvious (illustrated further in Figure 8a–c by the shading of $2\nu_{25}$, $2\nu_{26}$, and $\nu_{25} + \nu_{26}$ bands). When there is a large amount of Duschinsky mixing between two modes, the choice of the excited state labels becomes less clear. However, the S_1 assignment of the 175 cm^{-1} to 26^2_0 follows from the fact that it has the largest intensity in the ν_{26} progression. Similarly, the 462 cm^{-1} transition, which is assigned to 25^2_0 , has the largest FCF to 25^2_2 . Finally, the assignment of the 319 cm^{-1} transition to $25^1_0 26^1_0$ is straightforward since the frequencies of 26^2_0 and 25^2_0 are known.

Figure 8d–f presents the SVLF spectra from (d) 36^2_0 (at $+336\text{ cm}^{-1}$), (e) $35^1_0 36^1_0$ (at $+272\text{ cm}^{-1}$), and (f) 35^2_0 (at $+210\text{ cm}^{-1}$) transitions of *cc*-*m*DVB. As in the a_2 modes discussed above, these spectra share many transitions to the same ground state levels. All three spectra have in common a short progression in the b_1 -torsion with $2\nu_{36}$ and $4\nu_{36}$ at 86 and 186 cm^{-1} . In the SVLF of 36^2_0 , there is a strong band at 302 cm^{-1} that is assigned to $6\nu_{36}$. The b_1 -bend, ν_{35} , has its first overtone at 341 cm^{-1} , which is observed in all three SVLF spectra. This assignment is consistent with the 173 cm^{-1} calculated value for the ν_{35} . Consequently, the strong band at 207 cm^{-1} observed in all three SVLF spectra is readily assigned to $\nu_{35} + \nu_{36}$. The strong band at 309 cm^{-1} in the SVLF spectrum of $35^1_0 36^1_0$ and 35^2_0 is then $\nu_{35} + 3\nu_{36}$. This combination band is not cleanly resolved in the SVLF spectrum of 36^2_0 due to the strong transition at 302 cm^{-1} , which is assigned to $6\nu_{36}$. Likewise, $6\nu_{36}$ may be unresolved in the SVLF spectrum obtained by exciting the $35^1_0 36^1_0$ transition, due to the strong $\nu_{35} + 3\nu_{36}$ transition at 309 cm^{-1} .

As with the a_2 modes, the intensities in the cross-sequences observed in the SVLF of the combinations and overtones of the b_1 modes make the excited state labels less clear. However, the logical assignment of the 210 cm^{-1} transition is 35^2_0 since it has the largest FCF to 35^2_2 . It follows, then, that the two remaining transitions at $+272$ and $+336\text{ cm}^{-1}$ must be $35^1_0 36^1_0$ and 36^2_0 , respectively.

As is seen in the jet-cooled excitation spectrum of STY,⁵ in the $S_1 \leftarrow S_0$ excitation spectrum of *cc*-*m*DVB, the intensities of the combination bands of the bend + torsion are much larger than those of either the overtones of the bends and torsions themselves for both the a_2 and b_1 modes. However, in the 0^0_0 SVLF spectrum, the intensity of the overtones of the torsions is much larger than those due to either the overtone of the bend or the bend + torsion combination bands. This is another manifestation of the Duschinsky mixing. Moreover, the frequencies of the two torsions in *cc*-*m*DVB, ν_{26} and ν_{36} , increase by a factor of 2.5 – 3.5 in the excited state, while the b_1 -bend, ν_{35} , decreases by a factor of 1.6 . These changes in the excited state are consistent with STY whose bend decreases by a factor of ~ 2 and torsion increases by a factor of ~ 4 .² However, unlike in STY, the a_2 -bend, ν_{35} , increases only slightly in the excited state in *cc*-*m*DVB.

tt-*m*DVB and *t*-*p*DVB. As in *cc*-*m*DVB, in *tt*-*m*DVB and *t*-*p*DVB, the 0^0_0 SVLF (Figure 7c,d) and the $S_1 \leftarrow S_0$ excitation (Figure 6c,d) spectra are also dominated by totally symmetric in-plane fundamentals and combinations/even overtones of oop vibrations. Firm assignments of many of the transitions observed in the excitation spectra were made by taking SVLF from the corresponding transitions in both conformers. The frequencies of these transitions and the corresponding ground state transitions are given in Tables 2 and 3.

The remaining prominent features in the excitation spectra of *tt*-*m*DVB and *t*-*p*DVB are due to overtones and combination bands involving the oop torsions and bending modes. Figures

TABLE 4: Selected Low-Frequency Assignments of Transitions Observed in the SVLF Spectra Following Excitation of the Indicated Transitions of *cc-mDVB*

36^2_0		$35^1_036^1_0$		35^2_0	
$\Delta\nu$ (cm $^{-1}$)	mode	$\Delta\nu$ (cm $^{-1}$)	mode	$\Delta\nu$ (cm $^{-1}$)	mode
0	36^2_0	0	$35^1_036^1_0$	0	35^2_0
81	36^2_2	81	$35^1_036^1_2$	81	$35^2_036^0_2$
186	36^2_4	186	$35^1_036^1_4$	186	$35^2_036^0_4$
207	$35^0_136^2_1$	207	$35^1_136^1_1$	207	$35^2_036^0_1$
302	$35^0_136^2_3, 36^2_6$	309	$35^1_136^1_3, 35^1_036^1_6$	309	$35^2_036^0_3$
341	$35^0_236^2_0$	341	$35^1_236^1_0$	341	35^2_2
416–437	$35^0_136^2_5, 36^2_8, 35^0_236^2_2$	429	$35^1_136^1_5, 35^1_036^1_8, 35^1_236^1_2$	430	$35^2_036^2_2, 35^1_036^2_5$

26^2_0		$25^1_026^1_0$		25^2_0	
$\Delta\nu$ (cm $^{-1}$)	mode	$\Delta\nu$ (cm $^{-1}$)	mode	$\Delta\nu$ (cm $^{-1}$)	mode
0	26^2_0	0	$25^1_026^1_0$	0	25^2_0
56	26^2_2	56	$25^1_026^1_2$	247	$25^2_126^0_1$
130	26^2_4	130	$25^1_026^1_4$	309	$25^2_126^0_3$
214	26^2_6	214	$25^1_026^1_6$	390	$25^2_126^0_5$
247	$25^0_126^2_1$	247	$25^1_126^1_1$	439	25^2_2
308	$25^0_126^2_3$	308	$25^1_126^1_3$		
390	$25^0_126^2_5$	390	$25^1_126^1_5$		
439	$25^0_226^2_0$	439	$25^1_226^1_0$		

9 and 10 present the SVLF spectra from the combinations/overtones of oop transitions in *tt-mDVB* and *t-pDVB* that were useful in making ground state assignments of the oop torsions and bends. Frequencies of assigned transitions are listed in Tables 5 and 6. The FC activity, anharmonicity, and Duschinsky mixing observed in these spectra are similar to those in observed in STY^{2,3} and *cc-mDVB* and therefore will not be discussed further here.

ct-mDVB. The UVHB (Figure 6b) and 0^0_0 SVLF (Figure 7b) spectra of *ct-mDVB* are dominated by in-plane fundamentals. Frequencies of *ct-mDVB* fundamentals are given in Table 3. By comparison to *tt-* and *cc-mDVB*, *ct-mDVB* is of C_s rather than C_{2v} symmetry. Therefore, all in-plane fundamentals of *ct-*

mDVB are symmetry allowed. Furthermore, what used to be restricted to in-phase and out-of-phase motions of both vinyl groups in the other conformers may now be partially or completely localized on one or the other vinyl group.

Firm assignments to the a' fundamentals, 33^1_0 , 34^1_0 , 35^1_0 , and 37^1_0 , were made in a straightforward fashion from the SVLF spectra of these transitions. Additionally, assignments to 32^1_0 , 31^1_0 , 29^1_0 , and 23^1_0 were made by comparison to the frequency shifts and FC activity in *tt-m-*, *cc-m-*, and *t-pDVB*. Descriptions and frequencies of these transitions are given in Table 3.

Because of the small signal size of *ct-mDVB* relative to *cc-mDVB* and the number of overlapping bands with *cc-mDVB*, there is only one low-frequency band, at +266 cm $^{-1}$, in which a clean SVLF spectrum could be taken that is due to a combination of oop modes. Assignments to bands observed in

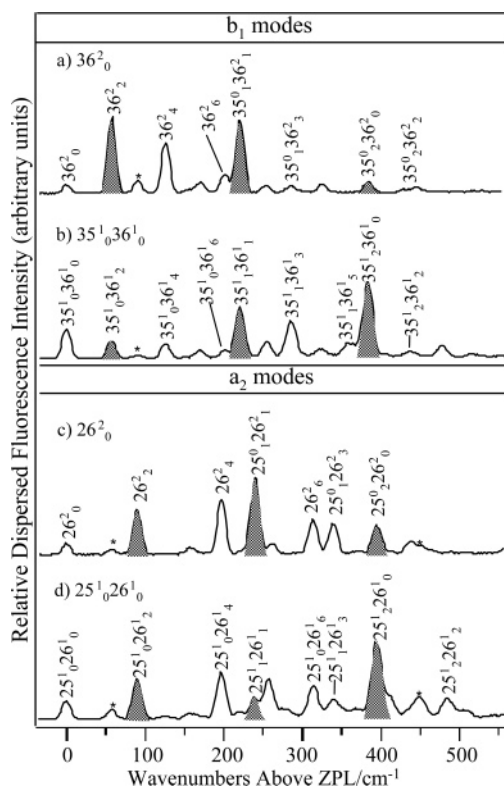


Figure 9. Assignments to out-of-plane vibrations observed in the SVLF of (a) 36^2_0 (at +128 cm $^{-1}$), (b) $35^1_036^1_0$ (at +275 cm $^{-1}$), (c) 26^2_0 (at +233 cm $^{-1}$), and (d) $25^1_026^1_0$ (at +276 cm $^{-1}$) bands of *tt-mDVB*.

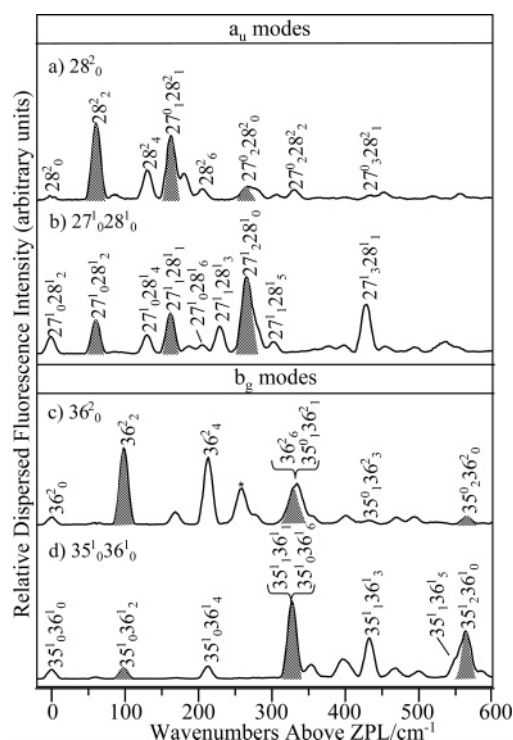


Figure 10. Assignments to out-of-plane vibrations observed in the SVLF of (a) 28^2_0 (at +113 cm $^{-1}$), (b) $27^1_028^1_0$ (at +210 cm $^{-1}$), (c) 36^2_0 (at +245 cm $^{-1}$), and (d) $35^1_036^1_0$ (at +376 cm $^{-1}$) of *t-pDVB*.

TABLE 5: Selected Low-Frequency Assignments of Transitions Observed in the SVLF of *tt*-mDVB

36^2_0		$35^1_036^1_0$		26^2_0		$25^1_026^1_0$	
$\Delta\nu$ (cm $^{-1}$)	mode	$\Delta\nu$ (cm $^{-1}$)	mode	$\Delta\nu$ (cm $^{-1}$)	mode	$\Delta\nu$ (cm $^{-1}$)	mode
0	36^2_0	0	$35^1_036^1_0$	0	26^2_0	0	$25^1_026^1_0$
57	36^2_2	57	$35^1_036^1_2$	57	$26^2_036^2_0$	57	$25^1_036^1_2$
90	$26^2_236^2_0$	90	$26^2_035^1_036^1_0$	90	26^2_2	90	$25^1_026^1_2$
126	36^2_4	126	$35^1_036^1_4$	197	26^2_4	197	$25^1_026^1_4$
202	36^2_6	202	$35^1_036^1_6$	240	$25^1_026^2_1$	240	$25^1_126^1_1$
220	$35^0_136^2_1$	220	$35^1_136^1_1$	314	26^2_6	314	$25^1_026^1_6$
285	$35^0_136^2_3$	285	$35^1_136^1_3$	340	$25^1_026^2_3$	340	$25^1_126^1_3$
356	$35^1_136^2_5$	356	$35^1_136^1_5$	395	$25^1_026^2_0$	395	$25^2_226^1_0$
384	$35^2_236^2_0$	384	$35^1_236^1_0$	449	$25^1_026^2_5(?)$	449	$25^1_126^1_5(?)$
434	$35^2_236^2_2$	434	$35^1_236^1_2$	483	$25^1_026^2_2$	483	$25^1_226^1_2$

TABLE 6: Selected Low-Frequency Assignments of Transitions Observed in the SVLF of *t-p*DVB

28^2_0		$27^1_028^1_0$		36^2_0		$35^1_036^1_0$	
$\Delta\nu$ (cm $^{-1}$)	mode	$\Delta\nu$ (cm $^{-1}$)	mode	$\Delta\nu$ (cm $^{-1}$)	mode	$\Delta\nu$ (cm $^{-1}$)	mode
0	28^2_0	0	$27^1_028^1_0$	0	36^2_0	0	$35^1_036^1_0$
60	28^2_2	60	$27^1_028^1_2$	98	36^2_2	98	$35^1_036^1_2$
130	28^2_4	130	$27^1_028^1_4$	213	36^2_4	213	$35^1_036^1_4$
162	$27^0_128^2_1$	162	$27^1_128^1_1$	259	$19^0_136^2_0$	336	$35^1_136^1_1, 35^1_036^1_6$
205	28^2_6	205	$27^1_028^1_6$	332	$35^0_136^2_1, 36^2_6$	432	$35^1_136^1_3$
265	$27^0_228^2_0$	229	$27^1_128^1_3$	432	$35^1_136^2_3$	549	$35^1_136^1_5$
330	$27^0_228^2_2$	265	$27^1_228^1_0$	565	$35^1_236^1_0$	565	$35^1_236^1_0$
428	$27^0_328^2_1$	301	$27^1_128^1_5$				
		428	$27^1_328^1_1$				

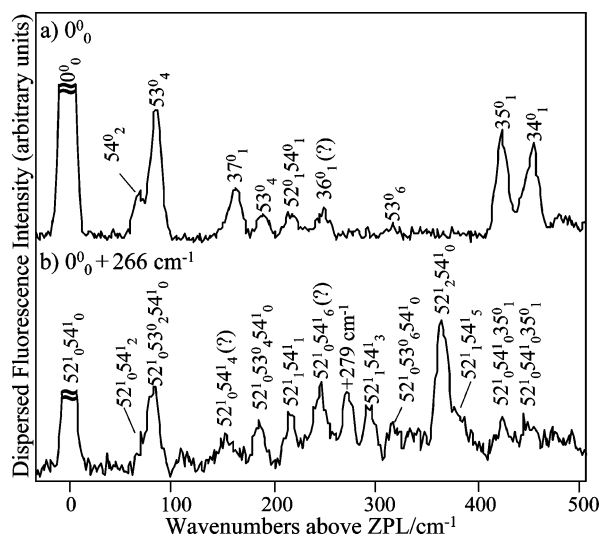
this spectrum are more complicated than in related SVLF spectra of *cc*- and *tt*-mDVB due to the increased number of cross-sequences observed in this lower symmetry isomer. The assignments that follow are necessarily tentative. However, it is worthwhile to discuss them for comparison to the other mDVB conformers.

The +266 cm $^{-1}$ SVLF spectrum is shown in Figure 11b along with the 0 0_0 SVLF (Figure 11a) for comparison. Both spectra have in common transitions at 87, 191, and 319 cm $^{-1}$, which by comparison to *cc*- and *tt*-mDVB, we assign to the short progression of ν_{53} (torsion of *cis*-vinyl group), with 2, 4, and 6 quanta, respectively. In the +266 cm $^{-1}$ SVLF spectrum, the strongest transition occurs at 367 cm $^{-1}$. This band is assigned to a transition to the first overtone of ν_{52} , the out-of-phase vinyl bend. The DFT calculated value of ν_{52} is 181 cm $^{-1}$. In both SVLF spectra there are also bands at 70 and 218 cm $^{-1}$, which are assigned to transitions to $2\nu_{54}$ (torsion of *trans*-vinyl group) and $\nu_{52} + \nu_{54}$, respectively. In accordance with the expected

anharmonicity in ν_{54} , the two bands at 297 and 384 cm $^{-1}$ in the +266 cm $^{-1}$ SVLF spectrum are assigned to $\nu_{52} + 3\nu_{54}$ and $\nu_{52} + 5\nu_{54}$. This leads to the assignment of the +266 cm $^{-1}$ band in the $S_1 \leftarrow S_0$ excitation spectrum to $52^1_054^1_0$. Therefore, the transition at 155 cm $^{-1}$ observed in the +266 cm $^{-1}$ SVLF spectrum is assigned to $52^1_054^1_4$.²⁰

c-pDVB. As mentioned above, there are bands in the UVHB spectrum of *pDVB* that do not holeburn out with *t-pDVB*. We have tentatively assigned these bands as belonging to *c-pDVB*. The furthest red-shifted transition, which occurs at 32 621 cm $^{-1}$, is tentatively assigned to the 0 0_0 transition of *c-pDVB*. The origin transition is not, however, the strongest transition observed. Two bands at 484 and 572 cm $^{-1}$ above the origin are much larger than the origin itself. These transitions probably gain intensity through vibronic coupling with the S_2 state. This notion is further supported by the predictions of Nguyen and co-workers¹⁰ that (by extension of Platt's rule) the transition dipole moment of *c-pDVB* lies along the *b*-axis and the S_1 state is a 1L_b state (the state of lower oscillator strength). If vibronic coupling with the 1L_a state is responsible for the two very intense transitions at 484 and 572 cm $^{-1}$ above the origin, then the corresponding vibrations must be of b_2 symmetry. DFT calculations predict two b_2 modes at 494 and 623 cm $^{-1}$ that we tentatively assign to the observed 484 and 572 cm $^{-1}$ bands. These modes are the $C_1-C_\alpha=C_\beta$ bend (27^1_0 in STY) and ring deformation (26^1_0 in STY and $6b^1_0$ in benzene), respectively.

Further support to these assignments is found if we look at other substituted benzenes, such as *p*-diethynylbenzene (*pDEB*), phenylacetylene (PA), and *o*-ethynylstyrene (*oES*), which all have strong vibronic coupling. In *pDEB* the strongest vibronically induced transition in the excitation spectrum is 20^1_0 at 492 cm $^{-1}$, where ν_{20} is the $C_1-C_\alpha=C_\beta$ bending mode.²¹ In PA, the corresponding mode is ν_{35} , and in the excitation spectrum of *oES*, a strong band at 537 cm $^{-1}$ is assigned as a vibronically induced transition, 28^1_0 , where ν_{28} is a ring angle bending mode corresponding to ν_{66} in benzene.⁷ In PA, the corresponding mode is ν_{34} , and in the

**Figure 11.** SVLF spectra from the (a) 0 0_0 and (b) 0 0_0 + 266 cm $^{-1}$ bands of *ct*-mDVB.

excitation spectrum of PA the 34^1_0 (at 556 cm^{-1}) transition is also vibronically induced.²²

3. Torsional Barrier Fitting. With many of the vinyl torsional levels in the conformers of *m*DVB assigned, it is a natural next step to use these energy levels to attempt a fit to a model two-dimensional potential for the torsional degrees of freedom of *m*DVB.

In order to assess the task before us, it is helpful to review briefly the way in which torsional energy levels have been used to determine one-dimensional potential functions for hindered rotation. Such fitting has been carried out successfully in molecules such as styrene, *o*-, *m*- and *p*-fluorostyrene, *p*-methoxystyrene, and *p*-methylstyrene.^{23–27} In *m*-fluorostyrene where the *cis* and *trans* conformers are spectroscopically distinguishable, the following potential form was used:²⁷

$$V(\theta) = \sum_{n=1-4,6} \frac{1}{2} V_n (1 - \cos(n\theta))$$

With this form of the potential, the barrier heights are determined by V_2 , while the V_1 and V_3 terms set the relative energies of the conformational minima. The V_4 term changes the shape of the conformer wells, flattening the bottom of the wells for small V_4 and producing a double minimum when $V_4 > 1/4 V_2$. The quality of the fit to such a potential form is improved as the number of torsional levels increases, thereby sampling levels nearer the top of the barrier. In *c-m*-fluorostyrene, torsional levels were observed up to about $1/3$ of the barrier height.²⁷ In such a circumstance, the energy levels are not yet perturbed by the presence of the other well. As a result, the relative energies of the *cis* and *trans* minima were poorly constrained. Thus, V_1 and V_3 in *c-m*-fluorostyrene were reported as ranges of possible values with large uncertainty in the relative energies of the minima. We anticipate a similar limitation in our 2D fitting in the absence of other constraints that set the relative energies of the minima.

The other point driven home by the styrene derivatives studied previously is the importance of having all the low-lying torsional levels assigned, including those that possess both even and odd numbers of torsional quanta. Since the vinyl torsion is an out-of-plane vibration, transitions involving the torsion appear in a vibronically resolved spectrum only with $\Delta v = \text{even}$ quantum number changes. Transitions beginning or ending in $v = \text{odd}$ then appear only via hot bands or sequence bands or in combination with another out-of-plane vibration of the same symmetry. In the absence of such data, there is a considerable uncertainty in the shape of the potential near the bottom of the well, since the same 0–2 spacing could be accommodated by different V_2/V_4 combinations that compensate for one another.

*m*DVB shares a planar equilibrium structure with the styrene derivatives studied previously.¹⁰ Under jet-cooled conditions, the vast majority of the population resides in the zero-point level in the ground state, and hence vibronic transitions to even-numbered quanta are observed. In the *cc* conformer, the 26^1_1 and $35^1_0 36^0_1$ hot bands were observable, establishing $v'' = 1$ in the ν_{26} and ν_{36} torsions. Furthermore, odd quanta of the torsions also appear in combination with the vinyl bends of the same symmetry. By assuming that the vinyl bends are harmonic, one can deduce the energies of the odd quanta torsional levels. These odd levels were included in the fit with an error twice that of the even quanta levels to account for uncertainties in the cross anharmonicities associated with the combination bands (Table 8). In the *tt* and *ct* wells, the analogous hot bands were not clearly assigned, leaving the odd quanta torsional levels more

TABLE 7: Fitting Parameters of the *m*DVB Potential Surface

parameters	fit of relaxed PES (cm^{-1})	fit to experiment (cm^{-1})	
	fit 1 ^a	fit 2 ^b	fit 3 ^c
V_2	1387	671 ± 30	695 ± 70
V_3	–15	-9 ± 6	16 ± 10
V_4	–258	-239 ± 11	-207 ± 30
V_{22}^c	14	-120 ± 20	-48 ± 35
V_{12}^c	2	-3 ± 1	15 ± 7
V_{22}^s	–1	-19 ± 2	43 ± 6
V_{12}^s	–2	11 ± 2	-50 ± 5
DFT symmetry		no	yes
1D barriers	1308–1367	904–920	754–828
2D barriers	2743–2790	1337–1340	1376–1405

^a Fit to the DFT computed relaxed PES. All error is less than 1 cm^{-1} .

^b Fit of the observed torsional levels without rotation of the wave functions. The indicated errors are one standard deviation, assuming uncorrelated parameters. V_2 , V_4 , and V_{cc}^2 are highly correlated. See text and Figure 13 for further discussion. ^c Fit of the observed torsional levels with rotation of the wave functions.

TABLE 8: Observed and Calculated Torsional Levels in *m*DVB

species-mode	transition	fit 2 calcd (cm^{-1}) ^d	fit 3 calcd (cm^{-1}) ^d	obsd data (cm^{-1})
<i>cc</i> - ν_{26}	0–1	29	27	27 ^a
	0–2	59	59	56
	0–3	95	94	88 ^c
	0–4	133	131	130
	0–5	172	170	170 ^c
	0–6	214	211	214
<i>cc</i> - ν_{36}	0–1	37	38	35 ^a
	0–2	80	82	81
	0–3	131	131	137 ^c
	0–4	186	184	186
<i>tt</i> - ν_{low}	0–1	26	17	27 ^b
	0–2	55	50	57
	0–3	90	88	92 ^c
	0–4	127	130	126
	0–5	166	175	163 ^c
<i>tt</i> - ν_{high}	0–6	207	223	202
	0–1	43	48	39 ^b
	0–2	90	94	90
	0–3	140	142	139 ^c
	0–4	195	190	197
<i>ct</i> - ν_{54}	0–1	27	26	31 ^b
	0–2	57	63	70
<i>ct</i> - ν_{53}	0–1	40	39	37 ^b
	0–2	86	84	86
average error		4%	7%	

^a Determined from hot bands. Observed error is twice that of known levels due to assumption of harmonic behavior required to determine the frequency of the hot bands. ^b Estimated values for $v = 1$ were used to constrain the fit to a near planar structure. The observed error is twice that of other known levels to account for the estimated value. ^c Estimated values from combination bands with the bend of the same symmetry and the value for the $v = 1$ level. The observed error is twice that of other known levels to account for the estimated value.

^d See Table 7 and the text for an explanation of fit 2 and fit 3.

poorly constrained than in *cc*, based only on combination bands with the vinyl bends. In attempts to constrain the fit to a planar structure,¹⁰ estimated values of the $v = 1$ levels in the *tt* and *ct* wells were included in the fit at twice the error of the even levels.

There are far fewer examples of two-dimensional torsional fitting in the literature. Most examples include two symmetric methyl rotors;²⁸ however, there are two examples of the two-dimensional torsional potential fitting for *trans*-stilbene that bear a closer resemblance to the present circumstance.^{29,30} In cases

where there are two symmetric rotors, the following potential form has been used,^{28–30}

$$V(\theta_1, \theta_2) = \sum_n \frac{1}{2} V_n (2 - \cos(n\theta_1) - \cos(n\theta_2)) + V_{12} (1 - \cos(n\theta_1) \cos(n\theta_2)) + V'_{12} (1 - \sin(n\theta_1) \sin(n\theta_2))$$

In *trans*-stilbene,²⁹ the potential function was fit using Meyer's two-dimensional flexible model.³¹ As a first step in the study of Orlandi et al.,²⁹ the terms of most importance were determined from fitting several points on a DFT computed relaxed PES. Once the form of the potential was in hand, then the observed torsional level structure could be fit to this potential form. In the case of *trans*-stilbene, the best-fit two-dimensional potential had the following form:²⁹

$$V(\theta_1, \theta_2) = \sum_{n=2,4} \frac{1}{2} V_n (2 - \cos(n\theta_1) - \cos(n\theta_2)) + V_{12} (1 - \cos(2\theta_1) \cos(2\theta_2))$$

with $V_2 = 1727(40)$, $V_4 = -447(12)$, and $V_{12} = 48(3)$.

In our study of *m*DVB we use the same approach. The 2D torsional potential for *m*DVB is somewhat more complicated than that in *trans*-stilbene because the vinyl groups themselves are asymmetric planar substituents, whereas the phenyl substituents in *trans*-stilbene are symmetric. As a result, there are three unique energies for the spectroscopically distinguishable minima: $V(cc) \neq V(tt) \neq V(ct) = V(tc)$. Furthermore, the first-order transition states fall into two inequivalent groups, with $V(dc) = V(uc) = V(cd) = V(cu)$, while $V(tu) = V(td) = V(dt) = V(ut)$, where "u" and "d" refer to up and down, respectively. In what follows, we will call these "1D-barriers" because the minimum energy pathway between conformational wells that traverses these transition states involves motion along only one of the torsional coordinates. Finally, isomerization from *cc* to *tt* along the $\theta_1 = \theta_2$ diagonal (a_2 symmetry axis) encounters the C_2 symmetry second-order transition state labeled *ud* or *du* (in which one vinyl group is above the plane and one is below), whereas isomerization along the $\theta_1 = -\theta_2$ diagonal (b_1 symmetry axis) encounters the C_s symmetry transition state (with both vinyl groups above or below the plane, labeled *dd* or *uu*).

In practice, the calculated asymmetry to the potential is quite small. For instance, the calculated energies of the C_2 (*ud*) and C_s (*uu*) transition states are within $\sim 7 \text{ cm}^{-1}$ of each other at $\sim 2800 \text{ cm}^{-1}$ ($\sim 2600 \text{ cm}^{-1}$ with ZPE), predicting that there is only small coupling between the two torsional motions. Furthermore, all of the first-order transition states are also very close in energy at about $\sim 1380 \text{ cm}^{-1}$ ($\sim 1280 \text{ cm}^{-1}$ with ZPE). Even the computed values of the *cc*, *tt*, and *ct* minima, which we have demonstrated to be spectroscopically distinguishable from one another, are quite close in energy with *tt* and *ct* ($=tc$) within $\sim 5 \text{ cm}^{-1}$ ($\sim 20 \text{ cm}^{-1}$ with ZPE) of each other and the *cc* minimum about $\sim 62 \text{ cm}^{-1}$ (75 cm^{-1} with ZPE) higher in energy.

Because there are three spectroscopically distinct conformational wells with unique torsional level spacing in each, the functional form we use for the 2D potential should be flexible enough to change the shape and relative energy of each well. At the same time, given our limited number of observed torsional levels, it is necessary to keep the number of terms in the potential as small as possible. In order to determine which terms are essential, we first carried out a fit to the calculated surface using the following general form, which retains the necessary symmetry with respect to exchange but assumes little

beyond this:

$$V(\theta_1, \theta_2) = \sum_{n,m} \frac{1}{2} V_n (2 - \cos(n\theta_1) - \cos(n\theta_2)) + V_{nm}^c (\cos(n\theta_1) \cos(m\theta_2) + \cos(m\theta_1) \cos(n\theta_2)) + V_{nm}^s (\sin(n\theta_1) \sin(m\theta_2) + \sin(m\theta_1) \sin(n\theta_2))$$

This fit included even and odd values of n up to 10 for the V_n terms and values of up to $n + m = 4$ for the cross terms. Of the "odd" V_n terms, only $n = 3$ was significantly different than zero, and the even terms above $n = 4$ are also small. The major cross terms are those with $n, m = 1-3$. The cross terms are also important in reshaping the wells to match the observed torsional level structure. In practice, it was possible to obtain a fit of good quality using only the V_{12} and V_{22} cross terms. As a result, a final fit to the calculated surface was carried out with the following form,

$$V(\theta_1, \theta_2) = \sum_{n=2-4} \frac{1}{2} V_n (2 - \cos(n\theta_1) - \cos(n\theta_2)) + V_{\text{cross}}$$

where

$$V_{\text{cross}} = V_{12}^c (\cos \theta_1 \cos 2\theta_2 + \cos 2\theta_1 \cos \theta_2) + V_{12}^s (\sin \theta_1 \sin 2\theta_2 + \sin 2\theta_1 \sin \theta_2) + V_{22}^c (\cos 2\theta_1 \cos 2\theta_2) + V_{22}^s (\sin 2\theta_1 \sin 2\theta_2)$$

The values of each parameter from the fit to the DFT potential surface are given in Table 7 (fit 1). With this fit in hand, the potential parameters from the fit were used as starting values in Meyer's flexible models program,³¹ which was adapted to a least-squares fitting routine to vary these potential parameters in order to best match the observed ground state torsional energies. In order to be sure that the computed energy levels were being compared with the correct experimental levels, assignments to each torsional level were made by analysis of the symmetries and nodal patterns of each level for each iteration. In the flexible model program a 13×13 grid size over the center of each well $\pm \pi/2$ was used with 35 energy levels calculated for each step (see ref 31 for a full explanation of the flexible models program). This grid size was chosen at the outset in order to maximize the efficiency of the calculations without compromising accuracy. The 13×13 grid provided a grid sufficiently closely spaced that the energy levels were unchanged with further increases in the number of grid points. As an additional check, once the best fit was obtained, a single point calculation at a 26×26 grid size was used to verify convergence.

When the initial values from the fit to the B3LYP/6-31+G* calculations were used as starting input for the fitting routine, the symmetries of the *cc* and *tt* torsional modes were inconsistent with the computed ordering based on the normal mode calculations. This inconsistency points out the difficulty in using a relaxed potential energy surface (which allows for energy optimization in all other degrees of freedom) as a starting point for match-up with either harmonic vibrational frequency calculations or experiment. At the same time, it is possible that the DFT B3LYP calculations do not predict the torsional frequencies to have the correct order. As a result, two fits were attempted, one ignoring the vibrational symmetry switch (by not reassigning the torsional levels during the fitting process, Table 7, fit 2) and one which required the torsional levels to have the symmetry/energy ordering as the DFT calculations (Table 7, fit 3).

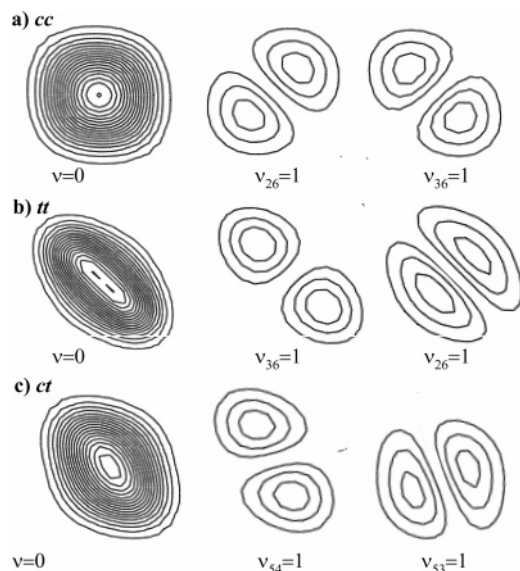


Figure 12. Contour plots of the $v = 0$ and $v = 1$ wave functions calculated from fit 3 illustrating the rotation of the wave functions in *cc*-, *tt*-, and *ct*-*mDVB*.

The fitting parameters of the first fit to the observed levels are given in Table 7 fit 2, and the frequencies are given in Table 8 fit 2. In this fit, the barriers for 1D-isomerization lie between 904 and 920 cm^{-1} , and the barriers along the diagonals are only about 400 cm^{-1} higher. The shape of the PES is quite different from the DFT B3LYP predictions where the diagonal barriers are approximately twice the 1D-barriers.

In fit 3 (Tables 7 and 8), where the normal mode calculated symmetries were required, the resulting form of the vibrations was correct in all three wells; that is, the best fit parameters properly accounted for the rotation of the vibrational wave functions in all three isomeric wells. In particular, the more nearly rectangular shape of the “*ct*” well results in a rotation of the normal mode directions to localize the two torsional modes on the inequivalent vinyl groups. The $v = 0$ and $v = 1$ wave functions for both torsional modes of each isomer are shown in Figure 12. In this fit, the barriers associated with the first-order transition states (e.g., “*cu*” or “*dt*”) are again much lower than the DFT calculations at 754–828 cm^{-1} ; however, the shape of the PES is more nearly similar to the predictions of the relaxed potential energy surface in that the diagonal barriers are about twice the 1D-barriers.

The errors listed in Table 7 are derived from χ^2 calculations assuming that the fit parameters V_2 , V_4 , and V_{22}^c are uncorrelated. However, the results from the gradient-based least-squares fitting routine indicate that these three parameters are highly correlated with one another, with a correlation parameter of -0.89 for V_2/V_4 , $+0.95$ for V_2/V_{22}^c , and -0.75 for V_4/V_{22}^c . In order to test the range of parameters that support torsional level structure that fit the observed levels near the experimental error, a series of single-point calculations were carried out over a grid of values about the “best fit” V_2 , V_4 , and V_{22}^c values. Figure 13 plots sets of potential parameters that had an average error in the 24 fit levels of less than 13% and a variance of less than 100 cm^{-2} . The linear plot links grid points that share the same V_{22}^c value, highlighting the linear correlation between V_2 and V_4 (with $V_4 = -0.26 V_2$). For the $V_{22}^c = 0$ line, the 1D barriers are given by V_2 , while the 2D barrier is $2V_2$. The important deduction to be drawn from these plots is that the observed torsional level structure can be fit by a rather wide range of

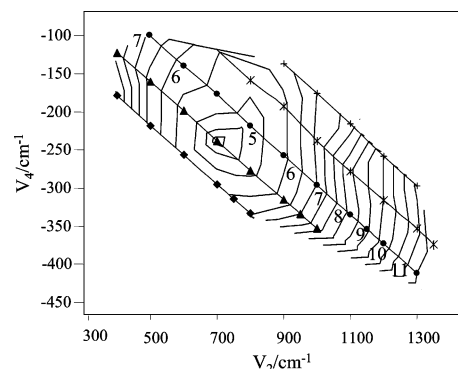


Figure 13. Plot of the acceptable sets of (V_2, V_4) values for (\blacklozenge) $V_{22}^c = -200 \text{ cm}^{-1}$, (\blacktriangle) $V_{22}^c = -100 \text{ cm}^{-1}$, (\bullet) $V_{22}^c = 0 \text{ cm}^{-1}$, (\ast) $V_{22}^c = 100 \text{ cm}^{-1}$, and ($+$) $V_{22}^c = 200 \text{ cm}^{-1}$ with contour plots shown of the average percent error of the fit to experiment. See the text for further discussion.

parameter sets associated with 1D barriers ranging from 500 to 1400 cm^{-1} .

Discussion and Conclusions

The purposes of this study were to find the “missing” conformations of *m*- and *pDVB*, to characterize the conformation specific ultraviolet spectroscopy of all the isomers in both the ground and the excited electronic states, and to determine the barrier to *cis* \rightarrow *trans* isomerization by fitting the C_1-C_α torsional levels to a two-dimensional potential form. The ultraviolet holeburning studies revealed that there are, indeed, three conformers of *mDVB* and two conformers of *pDVB* present in the supersonic expansion. These results are consistent with the predictions of DFT B3LYP calculations in that the energy differences in the three conformers of *mDVB* are small ($<75 \text{ cm}^{-1}$) and are likewise for the two conformers of *pDVB*.

The transitions due to the missing conformers have been found and assigned, and conformation-specific data are now available on the entire array of disubstituted isomers diethynylbenzene, ethynylstyrene, and divinylbenzene. The frequencies of the $S_1 \leftarrow S_0$ origins of the missing conformers fall into patterns that make sense relative to other members of this series (see Figure 10 in ref 8). In particular, in *mDVB*, the *tt*, *ct*, and *cc* conformers have $S_1 \leftarrow S_0$ origins at 32 164, 31 856, and 31 408 cm^{-1} , respectively. Thus, while the relative energies of the three conformers of *mDVB* are nearly isoenergetic in the ground electronic state (see the following paper), the *cc* and *ct* isomers are about 750 and 300 cm^{-1} more stable in S_1 than the *tt* conformer. Unfortunately, as was noted previously for the diethynylbenzenes,²¹ CIS calculations invert the order of the first two excited states relative to experiment, lending little confidence to such calculations providing the basis for an explanation of these trends. This would be a worthwhile subject of a future computational investigation.

The relative intensities of the transitions ascribable to both the “missing” *ct*-*mDVB* and *c*-*pDVB* isomers were much smaller than those of the other conformations (Figures 4 and 5). Initially, this was a puzzling result because the calculated energy differences for all the isomers are very small. As discussed above, in *c*-*pDVB* this reduced intensity in the R2PI spectrum may be explained by a smaller oscillator strength for the S_0-S_1 transition in *c*-*pDVB* than in *t*-*pDVB*. In fact, the small origin transition in *c*-*pDVB* is compensated by higher-lying vibronic transitions that are significantly larger than the tentatively assigned $S_1 \leftarrow S_0$ origin, presumably due to vibronic coupling to S_2 . This result was anticipated in the first studies

of the divinylbenzenes by Nguyen and co-workers.¹⁰ These authors noted that sizable changes in oscillator strength between conformers could occur because both the direction and magnitude of the transition dipole moments are affected by the relative position and orientation of the asymmetric vinyl substituents. This arises because of changes in the amount of electronic state mixing between the S_1 and S_2 states.

Similar reasoning could explain the weakness of the transitions due to *ct*-*m*DVB. Re-examination of the UVHB spectrum of *ct*-*m*DVB reveals that many of the vibronic transitions have intensities about half the size of the origin itself. In the other *m*DVB conformers, there is only one transition ($15^1_0/12^1_0$ in benzene) with this large an intensity compared to the origin transition, indicating that vibronic coupling may be playing a larger role in the spectrum of *ct* than the *cc* or *tt* isomers. Of course, the other logical reason for a small intensity for *ct*-*m*DVB is that it might have a smaller population than the other isomers. However, experiments are presented in the Supporting Information that show that the population of *ct*-*m*DVB is comparable to those of the other *m*DVB conformers, pointing back to oscillator strength arguments as the most likely explanation for the small intensities observed. It would be worthwhile to have a more complete theoretical description of the excited states of this series in order to explain the changes in oscillator strength that seem to be reflected in the data.

In large measure, the Franck–Condon activity observed in the R2PI spectra and dispersed fluorescence spectra of the isomers of *p*DVB and *m*DVB are similar to those anticipated of substituted benzenes. The most striking and useful aspect of the spectra presented here are the insights the low-frequency region of these spectra provide regarding the torsional and bending vibrations of the DVB isomers. Not surprisingly, the SVLF spectra from the overtones/combination bands involving the oop modes are very similar to styrene. These spectra are characterized by a negative anharmonicity in the torsions and strong Duschinsky mixing of the torsions and bending modes in the excited state.

A major focus of this work was to use the spectroscopic data available from the torsional level structure to map out a two-dimensional surface for isomerization along the two vinyl torsional coordinates θ_1 and θ_2 . In many ways, *m*DVB is a model system in which to pursue such a strategy by adding the complication of a second vinyl coordinate to a molecule (styrene) for which this strategy has already proven successful in one dimension.^{1–3} Unfortunately, the results of our fitting still leave considerable uncertainty to key elements of the 2D surface. In particular, the strong correlation between V_2 and V_4 shown in the linear plots of V_2 versus V_4 (in which $V_2/V_4 = -3.9$) indicates that the observed torsional levels determine a shape to the well but only very weakly constrain the true barrier heights ($V_{1D} = 500\text{--}1400\text{ cm}^{-1}$). Furthermore, the torsional data *within each well* cannot constrain the relative energies of the minima in any meaningful way. This points out the pressing need for an alternative method of determining barrier heights on potential energy surfaces. In the following paper, the lowest-energy isomerization barriers between all six reactant–product pairs of *m*DVB will be directly measured using the alternative method of stimulated emission pumping–population transfer spectroscopy.

Acknowledgment. The authors thank Rolf Meyer for sharing the flexible models program and for helping us with its implementation and gratefully acknowledge the support of the Department of Energy Basic Energy Sciences, Division of Chemical Sciences under Grant No. DE-FG02-96ER14656.

Supporting Information Available: Infrared hole-filling experiments that show the populations of the three *m*DVB conformers are approximately equal and SVLF scans of several bands in *m*DVB. This material is available free of charge via the Internet at <http://pubs.acs.org>.

References and Notes

- Hollas, J. M.; Ridley, T. *Phys. Chem. Lett.* **1980**, 94.
- Hollas, J. M.; Ridley, T. *J. Mol. Spectrosc.* **1981**, 89, 232.
- Hollas, J. M.; Musa, H.; Ridley, T.; Turner, P. H.; Weisenberger, K. H.; Fawcett, V. *J. Mol. Spectrosc.* **1982**, 94, 437.
- Ribblett, J. W.; Borst, D. R.; Pratt, D. W. *J. Chem. Phys.* **1999**, 111, 8454.
- Syage, J. A.; Adel, F. A.; Zewail, A. H. *Chem. Phys. Lett.* **1983**, 103, 15.
- Zwier, T. S. *J. Phys. Chem. A* **2006**, 110, 4133.
- Selby, T. M.; Zwier, T. S. *J. Phys. Chem. A* **2005**, 109, 8487.
- Selby, T. M.; Clarkson, J. R.; Mitchell, D.; Fitzpatrick, J. A. J.; Lee, H. D.; Pratt, D. W.; Zwier, T. S. *J. Phys. Chem. A* **2005**, 109, 4484.
- Selby, T. M.; Das, A.; Bekele, T.; Lee, H. D.; Zwier, T. S. *J. Phys. Chem. A* **2005**, 109, 8497.
- Nguyen, T. V.; Ribblett, J. W.; Pratt, D. W. *Chem. Phys.* **2002**, 283, 279.
- Clarkson, J. R.; Baquero, E.; Zwier, T. S. *J. Chem. Phys.* **2005**, 122, 214312.
- Dian, B. C.; Clarkson, J. R.; Zwier, T. S. *Science* **2004**, 303, 1169.
- Arrington, C. A.; Ramos, C.; Robinson, A. D.; Zwier, T. S. *J. Phys. Chem. A* **1998**, 102, 3315.
- Plusquellic, S. R.; Davis, S. R.; Jahanmir, F. *J. Chem. Phys.* **2001**, 115, 225.
- Majewski, W. A.; Meerts, W. L. *J. Mol. Spectrosc.* **1984**, 104, 271.
- Becke, A. D. *Phys. Rev. [Sect.] A* **1988**, 38, 3098.
- Lee, C.; Yang, W.; Parr, R. G. *Phys. Rev. [Sect.] B* **1988**, 37, 785.
- Frisch, M. J.; Pople, J. A.; Binkley, J. S. *J. Chem. Phys.* **1984**, 80, 3265.
- Frisch, M. J.; Trucks, G. W.; Schlegel, H. B.; Scuseria, G. E.; Robb, M. A.; Cheeseman, J. R.; Zakrzewski, V. G.; Montgomery, J. A., Jr.; Stratmann, R. E.; Burant, J. C.; Dapprich, S.; Millam, J. M.; Daniels, A. D.; Kudin, K. N.; Strain, M. C.; Farkas, O.; Tomasi, J.; Barone, V.; Cossi, M.; Cammi, R.; Mennucci, B.; Pomelli, C.; Adamo, C.; Clifford, S.; Ochterski, J.; Petersson, G. A.; Ayala, P. Y.; Cui, Q.; Morokuma, K.; Malick, D. K.; Rabuck, A. D.; Raghavachari, K.; Foresman, J. B.; Cioslowski, J.; Ortiz, J. V.; Stefanov, B. B.; Liu, G.; Liashenko, A.; Piskorz, P.; Komaromi, I.; Gomperts, R.; Martin, R. L.; Fox, D. J.; Keith, T.; Al-Laham, M. A.; Peng, C. Y.; Nanayakkara, A.; Gonzalez, C.; Challacombe, M.; Gill, P. M. W.; Johnson, B. G.; Chen, W.; Wong, M. W.; Andres, J. L.; Head-Gordon, M.; Replogle, E. S.; Pople, J. A. *Gaussian 98*, revision A.7; Gaussian, Inc.: Pittsburgh, PA, 1998.
- An alternative assignment is the combination band $52^1_053^1_054^1_2$. In both the 0^0_0 and the $52^1_054^1_0$ SVLF spectra there is a common transition at 250 cm^{-1} that maybe due to either ν_{36} (the out-of-phase in-plane vinyl bend) or to $6\nu_{54}$. It may be that in the 0^0_0 SVLF spectrum the 250 cm^{-1} band is 36^1_1 and in the $+266\text{ cm}^{-1}$ SVLF this band is due to both $52^1_054^1_036^1_0$ and $52^1_054^1_6$. This assignment would explain the small intensity of the 250 cm^{-1} band in the 0^0_0 SVLF spectrum and the larger intensity in the $52^1_054^1_0$ SVLF spectrum.
- Stearns, J. A.; Zwier, T. S. *J. Phys. Chem. A* **2003**, 107, 107117.
- King, G. W.; So, S. P. *J. Mol. Spectrosc.* **1971**, 37, 543.
- Hollas, J. M.; Bin Hussein, M. Z. *J. Mol. Spectrosc.* **1989**, 136, 31.
- Hollas, J. M.; Bin Hussein, M. Z. *J. Mol. Spectrosc.* **1991**, 145, 89.
- Hollas, J. M.; Taday, P. F. *J. Mol. Spectrosc.* **1992**, 153, 587.
- Ribeiro-Claro, P. J. A.; Teixeira-Dias, J. J. C.; Hollas, J. M.; Milewski, M. *J. Chem. Soc., Faraday Trans.* **1995**, 91, 197.
- Harper, C. M.; Hollas, J. M. *Chem. Phys. Lett.* **1994**, 226, 577.
- Durig, J. R.; Craven, S. M.; Harris, W. C. Determination of Torsional Barriers from Far-Infrared Spectra. In *Vibrational Spectra and Structure*; Durig, J. R., Ed.; Marcel Dekker: New York, 1972; Vol. 1; p 98.
- Orlandi, G.; Gagliardi, L.; Melandri, S.; Caminati, W. *J. Mol. Struct.* **2002**, 612, 383.
- Chiang, W.-Y.; Laane, J. *J. Chem. Phys.* **1994**, 100, 8755.
- Meyer, R. *J. Mol. Spectrosc.* **1979**, 76, 266.